Modelling, design and control of a bird neck using tensegrity mechanisms

A. Abourachid, C Böhmer, Philippe Wenger, Damien Chablat, Christine Chevallereau, Benjamin Fasquelle, Matthieu Furet

Modelling, design and control of a bird neck using tensegrity mechanisms

B. Fasquelle[1], M. Furet[1], A. Abourachid[2], C. Böhmer[2], D. Chablat[1], C. Chevallereau[1], P. Wenger[1],

***Abstract*— In birds, the neck exhibits remarkable performances and serves as a dextrous arm for performing various tasks. Accordingly, it is an interesting bioinspiration for designing new manipulators with enhanced performances. This paper proposes a preliminary bird neck model using several stacked tensegrity crossed bar mechanisms. It addresses several issues regarding kinetostatic and dynamic modelling, design and control.**

I. INTRODUCTION

The bird neck features outstanding dexterity and dynamic performances. Birds are capable of using their neck for dextrous tasks interacting with the environment (e.g. a vulture tearing food from a carcass), as well as for tasks demanding high force transmissions and accelerations (e.g. the woodpecker hitting a tree trunk). Contrary to hydrostats such as the elephant trunk or the cephalopod tentacle, bird necks have a spine that is composed of several elements (the vertebrae) like the snake. This work is carried out in the frame of the AVINECK project, a collaborative, multidisciplinary project with biologists and aims at proposing a bird neck robotic model. The concept of tensegrity has been chosen in this project as a general paradigm able to link the interests of biologists and roboticists. A tensegrity structure is made of compressive and tensile components held together in equilibrium [1], [2]. Tensegrity structures were first used in art [3] and have then been applied in civil engineering [4] and robotics [5], [6], [7], [8], [9], [10], [11], [12]. There are suitable to model muskuloskelet structures where the bones are the compressive components and the muscles and tendons are the tensile elements [13]. A preliminary, planar bird neck robotic model is considered in this paper. This model is built upon stacking a series of X-mechanisms i.e. crossed four-bar mechanisms with springs along their lateral sides. These mechanisms are inspired from the Snelson's X-shape mechanisms [2]. Although simplified due to its planarity, this model goes beyond the only available bird neck model in the literature that uses a simple planar articulated linkage [14], as it can be more easily actuated with cables that play the role of tendons and muscles. Snelson's X-shape mechanisms have been studied by a number of researchers, either as a single mechanism [5], [7], [15], [16] or assembled in series [17], [18], [9], [19], [20], [21]. In this paper, each X-shape mechanism is actuated with two lateral tendons threaded through the spring attachment points like in [9], [19], [20], and [21]. The resulting manipulator is supposed to operate in a vertical plane and is thus subject to gravity, unlike in [9], where the mechanism was used in a snake-like manipulator moving on the ground. This paper reports on some recent results obtained by our team on the AVINECK project.

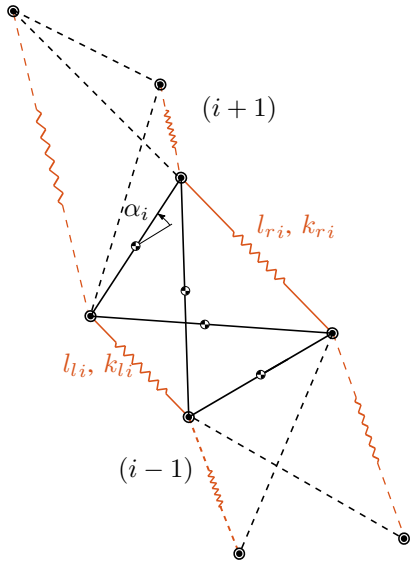

Fig. 1: Parametrization of a stack of mechanisms.

II. KINEMATIC AND DYNAMIC MODELLING

An assembly of N X-shape tensegrity mechanisms stacked in series is considered (see figure 1). The mechanisms i are numbered from $i = 1$ (base) to $i = N$ (head). Each mechanism i is a class-2 tensegrity mechanism [4] consisting of 3 bars and two pretensioned springs. The first mechanism is fixed to the ground and all the rigid links and springs are connected to each other with perfect revolute joints. Each X-mechanism i has a base bar and a top bar of length b and two crossed bars of length L (with the assembly condition $b \leq L$), thus defining an antiparallelogram. In parallel to the left spring (resp. to the right spring), a tendon (not shown in figure 1) applies a force f_{l_i} (resp. f_{r_i}).

If the position (x,y) of the end effector is defined in the middle of the top bar of the last mechanism, the direct kinematic model can be expressed as follows [20] [21]:

This work was conducted with the support of AVINECK Project ANR-16-CE33-0025

[1] Benjamin Fasquelle, Matthieu Furet, Damien Chablat, Christine Chevallereau and Philippe Wenger are with Laboratoire des Sciences du Numerique de Nantes, CNRS, Ecole Centrale de Nantes, France {Benjamin.Fasquelle, Matthieu.Furet, Christine.Chevallereau, Philippe.Wenger}@ls2n.fr

[2] Anick Abourachid and Christine Böhmer are with Museum National d'Histoire Naturelle, Paris, France abourach@mnhn.fr, boehmer.christine@gmail.com

$$\begin{cases} x = \sum_{i=1}^{n} l_i(\alpha_i)\cos(\frac{\pi-\alpha_i}{2} + \sum_{j=1}^{i} 2\alpha_j) \\ y = \sum_{i=1}^{n} l_i(\alpha_i)\sin(\frac{\pi-\alpha_i}{2} + \sum_{j=1}^{i} 2\alpha_j) \end{cases} \quad (1)$$

with:

$$l_i(\alpha_i) = l_{li} + l_{ri} = \sqrt{L^2 - b^2\cos^2(\frac{\alpha_i}{2})} \quad (2)$$

where α_i is the relative angle of the top bar of the mechanism i with respect to the top bar of mechanism $i-1$.

The dynamic model of the stacked mechanism is computed thanks to Lagrange's equations for a multi-dof (degree of freedom) system:

$$\frac{d}{dt}\left(\frac{\partial T}{\partial \dot{\alpha}_i}\right) - \frac{\partial T}{\partial \alpha_i} + \frac{dV}{d\alpha_i} + = Q_i, \qquad i = 1, 2, ..., n_{\text{dof}} \quad (3)$$

where T is the kinetic energy, V the potential energy, Q the generalized forces and n_{dof} is the number of dof (i.e the number of stacked X-mechanisms). The equation of motion can be written in the following form:

$$\mathbf{M}(\boldsymbol{\alpha})\ddot{\boldsymbol{\alpha}} + \mathbf{C}(\boldsymbol{\alpha}, \dot{\boldsymbol{\alpha}})\dot{\boldsymbol{\alpha}} + \mathbf{G}(\boldsymbol{\alpha}) = \mathbf{Q}(\boldsymbol{\alpha}) \quad (4)$$

where $\mathbf{M}$ is the inertia matrix, such that $T = \frac{1}{2}\dot{\boldsymbol{\alpha}}^\top \mathbf{M}\dot{\boldsymbol{\alpha}}$, $\mathbf{C}$ is the matrix of coriolis effects that can be deduced from $\mathbf{M}$ [22], $\mathbf{G}$ is the vector of potential effects, $\mathbf{G} = \frac{dV}{d\boldsymbol{\alpha}}$,and $\mathbf{Q}$ is the vector of generalized forces. In [23], the expression of $\mathbf{M}(\boldsymbol{\alpha})$, $\mathbf{G}(\boldsymbol{\alpha})$ are explicitly derived using an iterative procedure.

In this study, each mechanism is assumed fully actuated in an antagonist way, namely, a pair of tendons applies two positive forces f_{li} and f_{ri} in parallel to the left and right spring, respectively. The generalized forces vector $\mathbf{Q}$ defined in (3) is the torque associated to the generalized coordinate $\boldsymbol{\alpha}$:

$$\mathbf{Q} = \mathbf{Z}_l\mathbf{f}_l + \mathbf{Z}_r\mathbf{f}_r \quad (5)$$

with $\mathbf{f}_l = [f_{l1}, ..., f_{lN}]^\top$, $\mathbf{f}_r = [f_{r1}, ..., f_{rN}]^\top$, $\mathbf{Z}_l$ and $\mathbf{Z}_r$ are two diagonal matrices whose entries are respectively $-\frac{dl_{li}}{d\alpha_i}$ and $-\frac{dl_{ri}}{d\alpha_i}$, $i = 1, ..N$.

III. Control

Each mechanism i has a desired trajectory α_i^d. Let $\boldsymbol{\alpha}^d$ be the vector of all those trajectories, and $\boldsymbol{\alpha}$ the vector of the measured mechanism orientations. The control law is built from equation (4). Low velocities are assumed and the Coriolis effects are thus neglected: $\mathbf{C} = \mathbf{0}_{N\times N}$. Thus, the desired torque $\mathbf{Q}_d$ is:

$$\mathbf{Q}_d = \mathbf{M}(\boldsymbol{\alpha})\Big(\ddot{\boldsymbol{\alpha}}^d + k_d\mathbf{I}_N(\dot{\boldsymbol{\alpha}}^d - \dot{\boldsymbol{\alpha}}) + k_p\mathbf{I}_N(\boldsymbol{\alpha}^d - \boldsymbol{\alpha})\Big) + \mathbf{G}(\boldsymbol{\alpha}) \quad (6)$$

where k_d and k_p are the gains of the control law. The required forces $\mathbf{f}_l$ and $\mathbf{f}_r$ must satisfy:

$$\mathbf{Q}_d = \mathbf{Z}_l(\boldsymbol{\alpha})\mathbf{f}_l + \mathbf{Z}_r(\boldsymbol{\alpha})\mathbf{f}_r \quad (7)$$

The solution that minimizes the norm of the sum of the forces $||\mathbf{f}_l + \mathbf{f}_r||$ is chosen i.e. since forces must remain positive, for each mechanism one force is zero and the other one produces the motion.

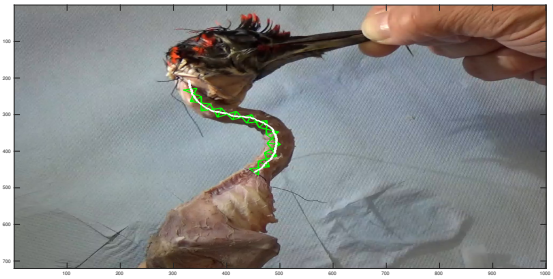

Fig. 2: First frame of the video, where the middle line of the neck is added in white, and the placed mechanisms are in green. The bird is a green woodpecker (*Picus viridis*).

IV. Extraction of a neck move from a video

Our goal is to reproduce movements made by a woodpecker with the proposed tensegrity manipulator. To get bird neck movements, recorded videos of bird movements would be used. However, on alive birds, the feathers around the neck make it almost impossible to distinguish the neck. The extraction of a move was made from a video of a bird corpse from which the feathers were removed, moved by hand.

The video was made with a green woodpecker.

The motion capture was performed frame by frame. For each frame, the line at the middle of the neck is detected and the mechanisms are then placed along this line.

A. Positioning the mechanisms along the line

To reproduce the neck trajectory with the tensegrity manipulator, the position of each mechanism at each frame is required. The number of mechanims N, the lengths of the top bars b_i and the diagonal bars L_i of each mechanism i are fixed. The orientation of the base of the neck γ_0 is given by the orientation of the string at this place. The middle of the base bar x_0 is given by the bottom of the middle line.

The mechanisms are placed one by one from the bottom. For each mechanism i, the orientation of the base bar γ_i and its center position x_i are given by

$$\gamma_i = \gamma_0 + \sum_{j=1}^{i-1} \alpha_j \quad (8)$$

$$x_i = x_0 + \sum_{j=1}^{i-1} \sqrt{L_j^2 - b_j^2 cos(\frac{\alpha_j}{2})^2} cos(\gamma_j + \frac{\alpha_j}{2}) \quad (9)$$

With a scan on the position α_i, a set of potential positions are tested. A mechanism is considered well positioned if the middle of its top bar is near the line and if the orientation of its top bar is near the perpendicular from the tangent to the line where the mechanism is located. Hence, the choosen position α_i is the one that minimizes the following function:

$$v(\alpha_i) = d(x_i) + \lambda|(\gamma_i + \alpha_i) - \alpha_{line}| \quad (10)$$

where $d(x_i)$ is the distance between the line and x_i, α_{line} is the angle of the perpendicular from the tangent to the line where the top bar of the mecanism cuts it, and λ is a parameter that can be used to modify the influence of the two parts.

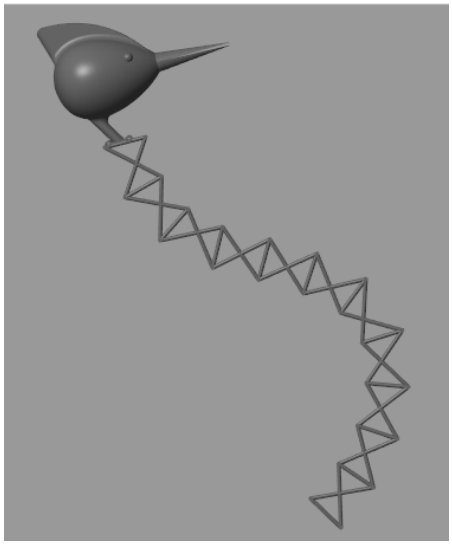

Fig. 3: The manipulator in Simscape. Only the solid bodies are visible.

B. Simulated movement

As the angle of the base of the neck does not change much during the video, it is fixed to $\gamma_0 = -\frac{\pi}{4}$. The manipulator is composed of $N = 11$ mechanisms, because the green woodpecker neck has 11 vertebrae. The $\frac{L}{b} = 1.52$ ratio is choosen by hand to have a manipulator with a size similar to the neck.

To define the trajectories of the mechanisms, the positions obtained previously were smoothed separately for each mechanism.

V. Simulation Results

A. Neck parameters

The manipulator studied is made of $N = 11$ identical mechanisms with $L = 0.152\,m$ and $b = 0.1\,m$. The springs free length is defined as $l_0 = L - b$ (which is the smallest length of the springs reached in the flat configurations $\alpha_i = \pm\pi$). All bars are cylinders of diameter $d = 0.01\,m$ and made of ABS with a volumic mass $1050\,kg/m^3$. All the springs have the same stiffness $k = 100N.m^{-1}$.

An head with a mass of $270g$ is put on the last mechanism. It is modelized like a sphere in the dynamic model. The Figure 3 shows the manipulator in Simscape. The cables and the springs are not observable.

The minimal and maximal bounds of the actuation forces are defined as $f_{min} = 0\,N$ (the tendons can only pull) and $f_{max} = 100\,N$, respectively.

B. Simulation results

Simulations are performed with Matlab Simulink and Simscape Multibody. Figure 4 shows the positions of the mechanisms during the simulation and the desired configuration based on the data extract for the video of the neck bird motion. The tracking is good and it has been shown in [23] that the use of the dynamic model allow to obtain better

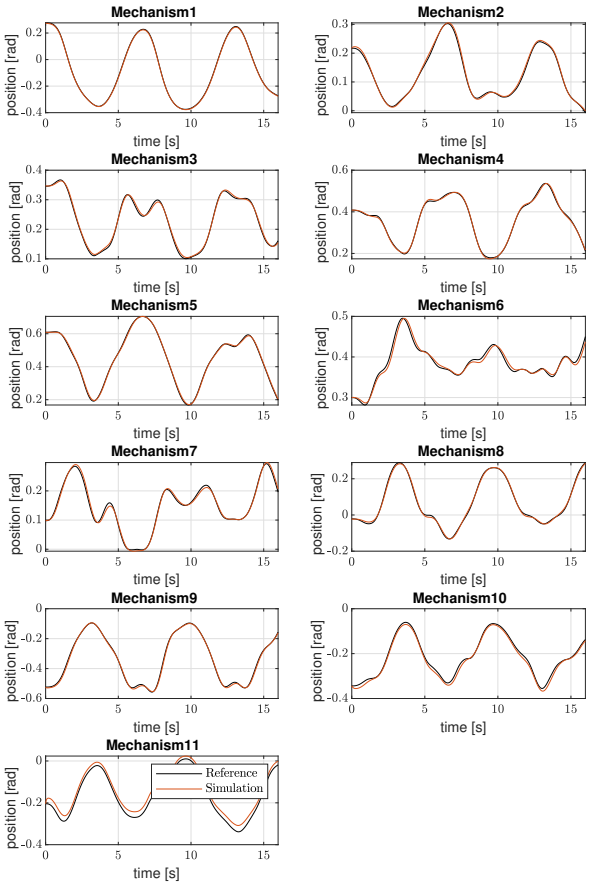

Fig. 4: Position during the simulations. The Reference curve (in black) corresponds to the desired trajectory, the red one is the result of the simulation.

result that a PD control law. The forces applied with the dynamic control law on each mechanism are shown in Figure 5. The present control law limits the forces applied by using only one antagonist actuator while the other one produces no force. A control of the stiffness of the mechanism can be also included to react to the environment.

VI. Conclusion and Perspectives

This paper analyzed the modeling, design and control of a tensegrity robot inspired from a bird neck and using a stack of X-shape tensegrity mechanism actuated by cables. The kinematic model was used to define a reference motion of each mechanism based on a video of the motion of a bird neck. The dynamic model was used to build a convenient control law to track the reference motion with an actuation composed of two independant forces acting on each mechanism.

A prototype is currently under development in order to carry out experimental work as illustrated in figure 6.

The current work concerns:

- The choice of the actuation,
- The interaction with the environment,

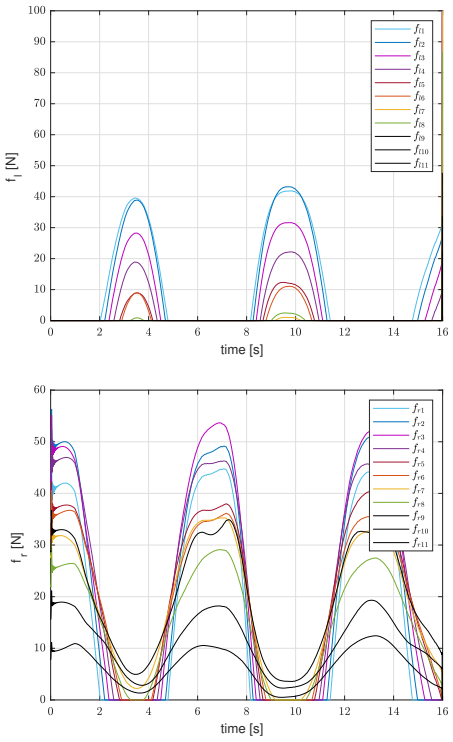

Fig. 5: Forces applied during the movement.

Fig. 6: The prototype under construction.

- The extension to 3D motion of each mechanism.

REFERENCES

[1] Motro, R. Tensegrity systems: the state of the art, Int. J. of Space Structures, 7 (2), pp 75–83, 1992

[2] K. Snelson, 1965, Continuous Tension, Discontinuous Compression Structures, US Patent No. 3,169,611

[3] R. B. Fuller, Tensile-integrity structures, United States Patent 3063521,1962

[4] Skelton, R. and de Oliveira, M., Tensegrity Systems. Springer, 2009

[5] M. Arsenault and C. M. Gosselin, Kinematic, static and dynamic analysis of a planar 2-dof tensegrity mechanism, Mech. and Mach. Theory, Vol. 41(9), 1072-1089, 2006

[6] C. Crane, J. Bayat, V. Vikas, R. Roberts, Kinematic analysis of a planar tensegrity mechanism with pres-stressed springs, in Advances in Robot Kinematics: analysis and design, pp 419-427, J. Lenarcic and P. Wenger (Eds), Springer (2008)

[7] P. Wenger and D. Chablat, Kinetostatic Analysis and Solution Classification of a Planar Tensegrity Mechanism, proc. 7th. Int. Workshop on Comp. Kinematics, Springer, ISBN 978-3-319-60867-9, pp422-431, 2017.

[8] Q. Boehler, M. Vedrines, S. Abdelaziz, P. Poignet, P. Renaud, Design and evaluation of a novel variable stiffness spherical joint with application to MR-compatible robot design. In Robotics and Automation (ICRA), 2016 IEEE International Conference on (pp. 661-667).

[9] D. Bakker, D. Matsuura, Y. Takeda, J. Herder, Design of an environmentally interactive continuum manipulator, Proc.14th World Congress in Mechanism and Machine Science, IFToMM'2015, Taipei, Taiwan, 2015

[10] J. Rieffel and J.B. Mouret, Adaptive and Resilient Soft Tensegrity Robots, Soft Robotics 2018 Jun 1; 5(3): 318–329.

[11] V. Baum, T. Kaufhold, I. Zeidis, K. Zimmermann, Spherical mobile robot based on a tensegrity structure with curved compressed members. AIM 2016: 1509-1514.

[12] M Vespignani, J. Friesen, V. SunSpiral, J. Bruce , Design of superball v2, a compliant tensegrity robot for absorbing large impacts. 2018 IEEE/RSJ International Conference on Intelligent Robots and Systems.

[13] S. Levin, The tensegrity-truss as a model for spinal mechanics: biotensegrity, J. of Mechanics in Medicine and Biology, Vol. 2(3), 2002

[14] G. Zweers, R. Bout, J. Heidweiller, Perception and Motor Control in Birds: An Eco- logical Approach. Springer, 1994, ISBN: 978-3-642-75869-0.

[15] Q. Boehler, I. Charpentier, M. Vedrines, P. Renaud, Definition and computation of tensegrity mechanism workspace, ASME J. of Mechanisms and Robotics, Vol 7(4), 2015

[16] A. Van Riesen, M. Furet, C. Chevallereau, P. Wenger, Dynamic Analysis and Control of an Antagonistically Actuated Tensegrity Mechanism, in Romansy 22 – Robot Design, Dynamics and Control, Spinger, ISBN: 978-3-319-78962-0, 2018

[17] JB Aldrich and RE Skelton, Time-energy optimal control of hyper-actuated mechanical systems with geometric path constraints, in 44th IEEE Conference on Decision and Control, pp 8246-8253, 2005

[18] S. Chen and M. Arsenault, Analytical Computation of the Actuator and Cartesian Workspace Boundaries for a Planar 2-Degree-of-Freedom Translational Tensegrity Mechanism, Journal of Mech. and Rob., Vol. 4, 2012

[19] M. Furet, A. Van Riesen, C. Chevallereau, P. Wenger, Optimal Design of Tensegrity Mechanisms Used in a Bird Neck Model, in EuCoMeS2018: Proceedings of the 7th European Conference on Mechanism Science, Springer, ISBN: 978-3-319-98019-95

[20] M. Furet, M. Lett, P. Wenger, Kinematic analysis of planar tensegrity 2-X manipulators, Proc. 16th International Symposium on Advances in Robot Kinematics, Bologna, Italia, 2018

[21] M. Furet and P. Wenger, Workspace and cuspidality analysis of a 2-X planar manipulator, Proc. 4th IFToMM Symposium on Mechanism Design for Robotics, Udine, Italia, 2018

[22] W. Khalil and E. Dombre, Modeling, identification and control of robots. HPS, 2002

[23] B. Fasquelle, M. Furet, C. Chevallereau, P. Wenger, Dynamic modeling and control of a tensegrity manipulator mimicking a bird neck, 15th IFToMM World Congress, Krakow, Poland, 2019